Journal of Materials and Electronic Devices 3 (2024) 1-7

Thermokinetic and Structural Shape Memory Effect Analysis of High-Temperature Martensitic Transformation of Ternary CuAlFe Alloy

Oktay KARADUMAN[1], İskender ÖZKUL[2], Yakup AYDEMİR[3], Canan Aksu CANBAY[3*]

[1]Rare Earth Elements Application and Research Center (MUNTEAM), Munzur University, 62000, Tunceli, TÜRKİYE
[2]Department of Mechanical Engineering, Faculty of Engineering, Mersin University, Mersin, TÜRKİYE
[3]Department of Physics, Faculty of Science, Firat University, 23119 Elazig, TÜRKİYE

Cu-based shape memory alloys (SMAs), the closest alternative SMA group to the superior but high-cost NiTi SMAs, can have possibilities for more microstructural optimisation for operating at high temperatures. In this work, the ternary CuAlFe high-temperature shape memory alloy (HTSMA) was fabricated by melting in an arc melter. The obtained alloy was homogenized and then quenched to build the martensite structure (shape memory mechanism) in the alloy texture. To investigate the shape memory characteristics of the CuAlFe alloy, differential scanning calorimetry (DSC) and differential thermal analysis (DTA) measurements were carried out to observe the thermally induced reversible martensitic phase transformations. To reveal the existence of the formed martensite phases in the alloy, X-ray diffraction (XRD) test was performed by using CuKα radiation at room temperature. The obtained all results revealed the high-temperature shape memory effect properties of the fabricated CuAlFe alloy. Therefore can be potentially beneficial in the HTSMA related research, development and application areas.

Keywords: *CuAlFe high-temperature shape memory alloy, Cu-based SMAs, Martensitic transformation, DSC, DTA, XRD*

Submission Date: 18 June 2024
Acceptance Date: 10 August 2024

**Corresponding author: caksu@firat.edu.tr*

1. Introduction

Since the first discovery of shape memory alloys (SMAs) in the mid of last century, these promising smart materials having unique functional shape memory effect (SME) and superelasticity (SE) properties, have been produced by different production methods and utilized in many technological and industrial application areas such as automotive, actuator, aero-space, medical, robotics, civil-engineering, energy harvesting/converting, textile, micro/nano electromechanic systems (M/NEMSs), or optoelectronic [1–16].

Among commercial SMAs, nickel-titanium (NiTi, or nitinol) SMAs are preferred to be used in most of applications [1,2,4–9,13–15,17–25] due to the superior shape memory and superelastic properties of these expensive SMAs. But, cost-effective Cu-based based SMAs, being nearly ten times cheaper than NiTi ones, are regarded the closest alternative to NiTi SMAs.

The working mechanism of shape memory effect property of SMAs is based on a solid-to-solid phase transition reaction called as martensitic transformation. Martensitic transformations, fundamentally induced by heat, occur reversibly, atomically non-diffusional and isostatically between two different solid phases of SMAs called as the product or martensite phase (low temperature phase) and the parent or austenite (high temperature phase) [2]. The martensitic transformation can be forward transformation

from austenite to martensite (A→M) on cooling a SMA or reverse transformation from martensite to austenite (M→A) on heating a SMA. For example, during cooling a NiTi SMA, when the temperature reaches down to a critical point, an austenite phase with cubic lattice structure can convert to a martensite phase with a monoclinic lattice structure, which is a forward or direct martensitic transformation [2,26]. The start and finish temperatures for the reverse transformation (transformation to austenite, M→A) and forward transformation (transformation to martensite, A→M) are denoted from the highest to the lowest as $A_f > A_s > M_s > M_f$, sequentially. Transformation to each one of these solid phases completes at their finish temperatures (A_f or M_f). If a SMA is plastically bended (permanently deformed) when it is in martensite phase (at below M_f) and then heated up to above A_f, the SMA will get austenite phase and (original) shape by heat-induced internal stresses forcing crystal structure (unit cell) of martensite transform into crystal structure of austenite. The sum of all microscale shape (geometric) change of unit cells of deformed martensite in such transformation to the first original (austenite) shape can be eye-seen as a macroscopic shape change.

Studies on polycrystalline Cu-based SMAs have still been made without cutting pace to modify their SME, SE or damping properties and/or to improve their disadvantages such as their brittleness, and thermal instability (instability of martensite or austenite phases) that affects transformation temperatures, hysteresis, strain recovery i.e. their shape memory properties.

SMAs with high working (transformation) temperatures, called as high-temperature shape memory alloys (HTSMAs), are demanded in many related applications such as robotics, aerospace, automotive or power generation [18]. Some NiTi-, Ti-, Ni-, Zr-, or Ru-based HTSMA systems [18,27,28] have already been studied until today. However, Cu-based HTSMAs [29–32] are cost-effective and can exhibit higher transformation temperatures and also they show easier processing performance that is good to manufacture parts with complex structures [30]. Therefore, they atracts researchers to investigate on them and to improve or modify their properties.

Generallly, CuAlNi and CuAlFe HTSMAs with relatively good SME are two main group of Cu-based HTSMAs showing transformation temperatures above 200 °C that can be adjusted in a range between 100 and 500 °C [27,30]. CuAlFe HTSMAs can show higher transformation temperatures than CuAlNi ones [30]. However, CuAlFe HTSMAs still need to be more investigated, especially to study on their thermodynamic shape memory properties and to obtain different transformation temperatures.

In this work, the ternary CuAlFe high-temperature shape memory alloy (HTSMA) with 67.98Cu-27.51Al-4.52Fe (at%) was fabricated by arc melting method and its SME properties were investigated by thermal and structural tests.

2. Experimental Work

The ternary CuAlFe high-temperature shape memory alloy (HTSMA) with 67.98Cu-27.51Al-4.52Fe (at%) composition was fabricated by melting the pelletized powder mixture of high purity (%99.9) elements of Cu, Al, and Fe in a vacuum arc melter. After obtained the arc-melted ingot alloy, the ingot was cut into small test samples and then were homogenized at 900 ºC for 1 hour and immediately quenched in iced-brine water (in order to form martensite phase in the alloy by this rapid cooling). The differential scanning calorimetry (DSC) tests were carried out by using a Shimadzu 60A label DSC instrument at different 15, 20, 25 and 30 °C/min of heating/cooling rates under an inert argon gas flow of 100 ml/min to reveal the thermally induced shape memory effect behavior of the produced alloy. The differential thermal analysis (DTA) test was taken under same inert gas flow and at a single 25 °C/min of heating/cooling rate between room temperature and 900 °C by using a Shimadzu DTG-60AH instrument for behavior of the alloy at high temperatures. X-ray diffraction (XRD) pattern was obtained at room temperature via a Rigaku Miniflex 600 model X-ray diffractometer (by using CuKα X-rays) in order to reveal the formed martensite phases in the alloy matrix. EDS (energy dispersive X-ray spectrum) analysis was made to detect the alloy composition of the CuAlFe HTSMA by using a SEM-Hitachi SU3500 instrument at room temperature.

3. Results and Discussion

The DSC curves of the CuAlFe HTSMA obtained at different heating/cooling rates are given in Fig.1.

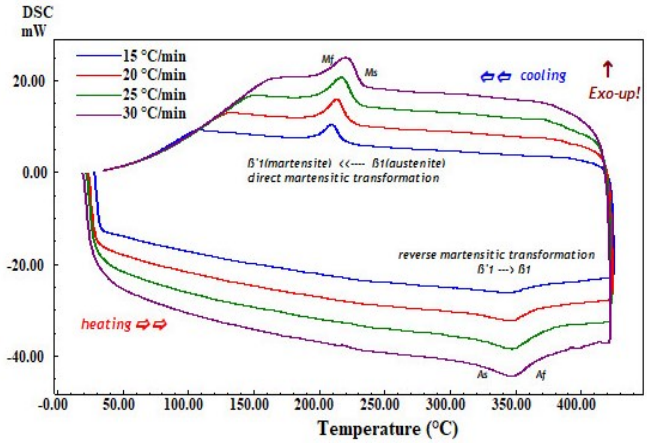

Fig.1. The DSC curves of the CuAlFe HTSMA show the down endothermic and up exothermic peaks indicating the reversible martensitic phase transformation peaks.

These looping DSC thermograms (curves) show the down endothermic phase transition peaks on their heating parts and up exothermic peaks on their cooling parts, which in turn indicate the reverse (M→A) and forward (A→M) martensitic phase transformation peaks of the CuAlFe HTSMA at high temperatures above 200 °C.

The characteristic martensitic transformation temperatures (A_s, A_f, A_{max}, M_s, and M_f) and the thermodynamic reverse (M→A) transformation enthalphy change ($\Delta H_{M\rightarrow A}$) values of the fabricated CuAlFe HTSMA were directly determined from the DSC peak analyses data obtained by applying tangent method and these are all given in Table 1. Also in this table, the given values of the thermal equilibrium temperature (T_0), i.e. at where there is no any driving force leading to a martensit transformation since the Gibbs (chemical) free energies of martensite and austenine phases are equalized at this temperature, were calculated by using Tong-Wayman formula [11,33] below;

$$T_o = \frac{1}{2}(A_f + M_s) \quad (1)$$

Table 1: The characteristic martensitic transformation temperatures and thermodynamic parameters of the CuAlFe HTSMA obtained from the DSC peak analyses data.

Heating/cooling rate (°C/min)	A_s (°C)	A_f (°C)	A_{max} (°C)	M_s (°C)	M_f (°C)	A_s-M_f (°C)	T_0 (°C)	$\Delta H_{M\rightarrow A}$ (J/g)	$\Delta S_{M\rightarrow A}$ (J/g°C)
15	317.36	363.82	342.95	219.54	198.05	119.31	291.68	8.97	0.0308
20	314.48	360.04	344.05	224.19	199.50	114.98	292.12	11.05	0.0378
25	318.44	369.73	347.56	229.37	200.78	117.66	299.55	11.00	0.0367
30	317.38	362.58	346.39	233.29	200.10	117.28	297.94	12.18	0.0409
Avg.	316.92	364.04	345.24	226.60	199.61	117.31	295.32	10.80	0.0365

The values of another thermodynamic parameter, the reverse transformation entropy ($\Delta S_{M\rightarrow A}$) change, also given in Table 1, were calculated by substituting the enthalpy change values in the formula given as below;

$$\Delta S_{M\rightarrow A} = \frac{\Delta H_{M\rightarrow A}}{T_o} \quad (2)$$

Apart from these, one another thermodynamic parameter, the activation energy (E_a) value of the reverse martensitic phase transition reaction of the fabricated CuAlFe HTSMA was calculated, too. E_a energy is an important reaction kinetic parameter in formation of martensitic transformation and it affects on the crystallization behavior of the alloy. Since martensitic phase transitions are first-order reactions, to calculate the E_a value of the CuAlFe HTSMA the formula of Kissinger [26,34] can be properly used as expressed below;

$$\frac{d\left[ln\left(\frac{\phi}{T_m^2}\right)\right]}{d\left(\frac{1}{T_m}\right)} = -\frac{E_a}{R} \quad (3)$$

here; ϕ refers to heating/cooling rate of DSC test, T_m represents the maximum peak temperature (A_{max}) of transformation and R is the universal gas constant (R=8.314 J/mol.K). The fraction term in the left side of Eq.3 expressing the change of activation energy is determined as the slope value obtained by linear-fitting $ln(\Phi/T_m^2)$ vs. $1000/T_m$ plot given in Fig.2. By substituting this slope value in Eq.3, the The Ea activation energy value for the reverse martensitic phase transition of the produced CuAlFe HTSMA was found as 381.08 kJ/mol.

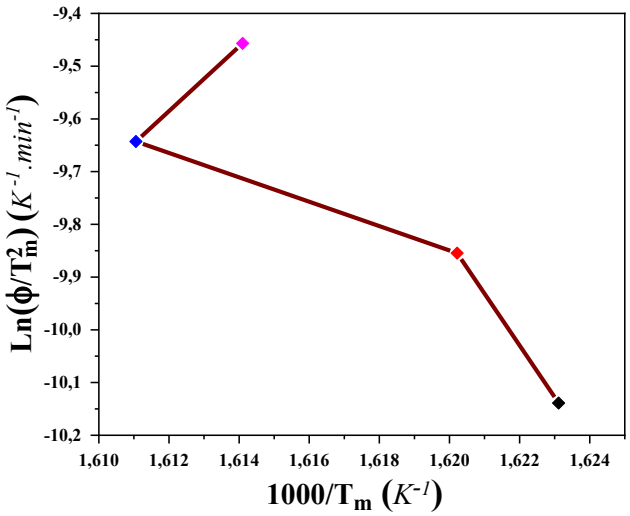

Fig.2. The activation energy change plot of the CuAlFe HTSMA.

The DTA curve of the CuAlFe HTSMA obtained at 25 °C/min of heating/cooling rate presented in Fig.3 shows the other thermally induced reactions in the CuAlFe HTSMA at high temperatures and also shows the reversible martensitic tansformation peaks again. The multiple peaks formed on the down side heating part of this DTA curve indicate a multiple phase transition chain and sequentally from far left

to the far right these peaks are the transitions as follows: martensite (β1′) →austenite (β1; DO_3 or $L2_1$) → B2 (metastable cubic) → precipitating → eutectoid dissolution → B2 (ordered cubic) →A2 (disordered cubic). This phase transitions chain is seen commonly in Cu-based SMAs [11,29,35–37].

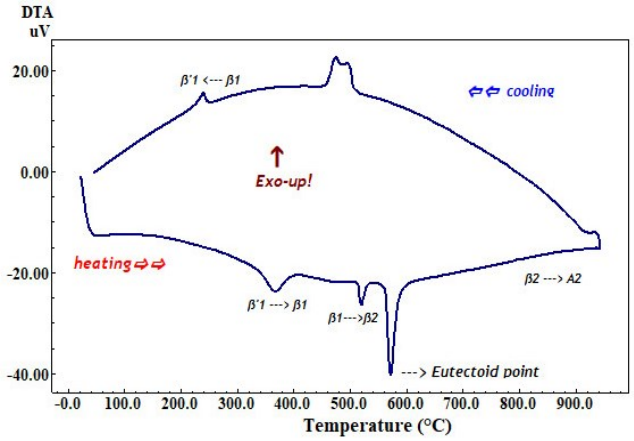

Fig.3. The DTA heating/cooling curve loop taken at single 25 °C/min of heating/cooling

The e/a ratio (average valence electron concentration per atom ratio) of the CuAlFe alloy was calculated as 1.596 by using the atomic fractions of the alloying elements constituting the 67.98Cu-27.51Al-4.52Fe (at%) composition of the alloy determined by the EDS test in the customized formula [11,29] given as below;

$$\frac{e}{a} = f_{Cu}v_{Cu} + f_{Al}v_{Al} + f_{Fe}v_{Fe} \quad (4)$$

here; f refers to the atomic fractions of the alloying elements, and v represents the corresponding valence electron numbers (here; v_{Cu} =1, v_{Al}=3, and v_{Fe}=2) of these elements. The e/a ratio of the CuAlFe alloy is found above the e/a ratio range of 1.45-1.51 which range is expressed as a theoretical condition for Cu-based alloys to have most probably a shape memory effect [2,29]. Moreover, Cu-based SMAs with e/a ratios in or close to this range can have two different martensite forms (β1′ and γ1′) together. The e/a value of the CuAlFe alloy found as 1.596 indicates that the γ'1(2H) type martensite phase must be formed dominantly over and together with the β'1(18R) type martensite in the produced CuAlFe memory alloy [29,35,38]. To confirm the presence of these martensite phases, the XRD test result of the alloy is given below.

The XRD pattern of the CuAlFe HTSMA given in Fig.4 displays the peaks indicating the presence of the monoclinic β1′(18R) and orthorhombic or hexagonal γ1′(2H) type martensite phases formed in the alloy at room temperature by the effect of rapid cooling (at the end of quenching). As seen on this pattern, the main XRD peak with the highest intensity is β1′(128) martensite peak, and the others are also some β1′ and some γ1′ type martensite peaks [27,29,39–41]. As seen on the XRD pattern of the CuAlFe alloy, as if the β1′ peaks are the dominant martensite peaks. However, according to the e/a value of the CuAlFe alloy, the γ1′ peaks were normally expected to be observed as the dominant, i.e. to be more intense and no fewer than the β1′ peaks. The cause of this is resulted from that the 2H hexagonal martensite has lesser symmetry (or more amorphism) than the monoclinical 18R martensite and also from the selected X-ray test area of the alloy surface [11]. The sum of coherently scattered X-rays or the scattering domain (spherical or ellipsoidal particle) size of 2H martensite is smaller than that of 18R martensite (the hexagonal 2H phase scatters fewer X-rays than a monoclinical 18R phase and it also absorbes less) [11].

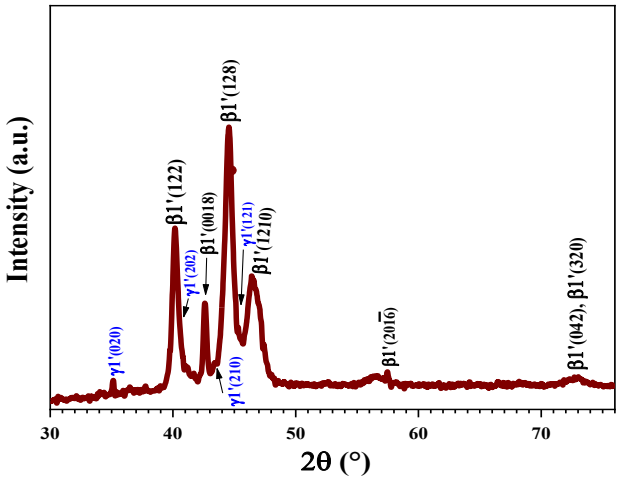

Fig.4. The XRD pattern of the CuAlFe HTSMA shows the co-existence of β1′ (18R) and γ1′ (2H) types of martensite phases.

By using XRD data of the main peak, the crystallite size (D) of the CuAlFe HTSMA was determined by using Debye-Scherrer formula [26,42] as given below;

$$D = \frac{0.9\lambda}{B_{\frac{1}{2}} \cos\theta} \quad (5)$$

here; λ stands for the wavelength of the CuKα X-ray (λ= 0.15406 nm), $B_{1/2}$ refers to the full width at half maximum (FWHM) value belongs to the highest (main) peak, and θ represents the Bragg angle of X-ray diffraction. The crystallite size (D) of the CuAlFe HTSMA was found as 11.27 nm.

4. Conclusions

The ternary Cu-Al-Fe HTSMA was fabricated succesfully by arc melting and the characterization tests of the alloy was made by differential calorimetry (DSC, DTA) and structural (XRD, EDS) measurements to investigate the shape memory

effect characteristics of the CuAlFe alloy. The calorimetry tests (DSC and DTA) results showed the stable and powerful peaks indicating the reversible martensitic transformations at the temperatures approximately in between 198 °C and 369 °C, and also the DTA curve on heating showed the multiple phase transitions chain of β1′(or β1′+γ1′) → β1(DO_3 or $L2_1$) → B2 → A2 which is common to the Cu-based shape memory alloys. The XRD pattern revealed the β1′and γ1′ types of martensites co-existing in the alloy, so that existence of a crystallographic base mechanism needed for the CuAlFe HTSMA to have its shape memory effect property was confirmed. The thermodynamic characterization of shape memory effect features of the fabricated CuAlFe alloy and other findings obtained in this work can be notably useful in HTSMA related research, development and applications.

Acknowledgments:

This research work is a part of thesis works of Yakup AYDEMİR mastering in general physics in Physics Department, Science Faculty, Firat University. Firat University Scientific Research Projects (FUBAP) financially supports this research work: FF.23.17 project number.

References:

[1] Fernandes DJ, Peres R V., Mendes AM, Elias CN. Understanding the Shape-Memory Alloys Used in Orthodontics. ISRN Dent 2011;2011:1–6. https://doi.org/10.5402/2011/132408.

[2] Otsuka K, Wayman CM. Shape memory materials. Cambridge University Press; 1999.

[3] Muthukumarana S, Messerschmidt MA. Clothtiles: A prototyping platform to fabricate customized actuators on clothing using 3d printing and shape-memory alloys. Conference on Human Factors in Computing Systems - Proceedings 2021. https://doi.org/10.1145/3411764.3445613.

[4] Concilio A, Antonucci V, Auricchio F, Lecce L, Sacco E (Eds.). Shape Memory Alloy Engineering. 2nd ed. Elsevier; 2021. https://doi.org/10.1016/C2018-0-02430-5.

[5] Riccio A, Sellitto A, Ameduri S, Concilio A, Arena M. Shape memory alloys (SMA) for automotive applications and challenges. Shape Memory Alloy Engineering: For Aerospace, Structural, and Biomedical Applications 2021:785–808. https://doi.org/10.1016/B978-0-12-819264-1.00024-8.

[6] Rao A, Srinivasa AR, Reddy JN. Design of Shape Memory Alloy (SMA) Actuators. Cham: Springer International Publishing; 2015. https://doi.org/10.1007/978-3-319-03188-0.

[7] Rao A, Srinivasa AR, Reddy JN. Introduction to shape memory alloys. SpringerBriefs in Applied Sciences and Technology 2015:1–31. https://doi.org/10.1007/978-3-319-03188-0_1.

[8] Hartl DJ, Lagoudas DC. Aerospace applications of shape memory alloys. Proceedings of the Institution of Mechanical Engineers, Part G: Journal of Aerospace Engineering 2007;221:535–52. https://doi.org/10.1243/09544100JAERO211.

[9] Fu YQ, Luo JK, Flewitt AJ, Huang WM, Zhang S, Du HJ, et al. Thin film shape memory alloys and microactuators. Int J Computational Materials Science and Surface Engineering 2009;2:208–26. https://doi.org/10.1504/IJCMSSE.2009.027483.

[10] Karaduman O, Canbay CA, Dere A, Orman Y, Al-Ghamdi AA, Al-Sehemi AG, et al. Smart alloy metalized novel photonic NEMS photodiode with CuAlV/n-Si/Al junction structure. Phys Scr 2024;99. https://doi.org/10.1088/1402-4896/ad2047.

[11] Canbay CA, Karaduman O. The photo response properties of shape memory alloy thin film based photodiode. J Mol Struct 2021;1235:130263. https://doi.org/10.1016/J.MOLSTRUC.2021.130263.

[12] Ayyıldız E, Türüt A. The effect of thermal treatment on the characteristic parameters of Ni/-, Ti/- and NiTi alloy/n-GaAs Schottky diodes. Solid State Electron 1999;43:521–7. https://doi.org/10.1016/S0038-1101(98)00287-1.

[13] Mohd Jani J, Leary M, Subic A, Gibson MA. A review of shape memory alloy research, applications and opportunities. Mater Des 2014;56:1078–113. https://doi.org/10.1016/j.matdes.2013.11.084.

[14] Mwangi JW, Nguyen LT, Bui VD, Berger T, Zeidler H, Schubert A. Nitinol manufacturing and micromachining: A review of processes and their suitability in processing medical-grade nitinol. J Manuf Process 2019;38:355–69. https://doi.org/https://doi.org/10.1016/j.jmapro.2019.01.003.

[15] Hite N, Sharar DJ, Trehern W, Umale T, Atli KC, Wilson AA, et al. NiTiHf shape memory alloys as phase change thermal storage materials. Acta Mater 2021;218. https://doi.org/10.1016/j.actamat.2021.117175.

[16] Mohamed ASY. Smart Materials Innovative Technologies in architecture; Towards Innovative design paradigm. Energy Procedia, vol. 115, Elsevier Ltd; 2017, p. 139–54. https://doi.org/10.1016/j.egypro.2017.05.014.

[17] Nespoli A, Passaretti F, Szentmiklósi L, Maróti B, Placidi E, Cassetta M, et al. Biomedical NiTi and β-Ti Alloys: From Composition, Microstructure and Thermo-Mechanics to Application. Metals (Basel) 2022;12:406. https://doi.org/10.3390/met12030406.

[18] Ma J, Karaman I, Noebe RD. High temperature shape memory alloys. International Materials Reviews 2010;55:257–315. https://doi.org/10.1179/095066010X12646898728363.

[19] Firstov GS, Van Humbeeck J, Koval YN. High-temperature shape memory alloys. Materials Science and Engineering: A 2004;378:2–10. https://doi.org/10.1016/j.msea.2003.10.324.

[20] Sutapun B, Tabib-Azar M, Huff MA. Applications of shape memory alloys in optics. Appl Opt 1998;37:6811–5. https://doi.org/https://doi.org/10.1364/AO.37.006811.

[21] Copaci D-S, Blanco D, Martin-Clemente A, Moreno L. Flexible shape memory alloy actuators for soft robotics: Modelling and control. Int J Adv Robot Syst 2020;17:1–15. https://doi.org/10.1177/1729881419886747.

[22] Wen C, Yu X, Zeng W, Zhao S, Wang L, Wan G, et al. Mechanical behaviors and biomedical applications of shape memory materials: A review. AIMS Mater Sci 2018;5. https://doi.org/10.3934/matersci.2018.4.559.

[23] Eschen K, Granberry R, Abel J. Guidelines on the design, characterization, and operation of shape memory alloy knitted actuators. Smart Mater Struct 2020;29:035036. https://doi.org/10.1088/1361-665X/ab6ba7.

[24] Costanza G, Tata ME. Shape Memory Alloys for Aerospace, Recent Developments, and New Applications: A Short Review. Materials 2020;13. https://doi.org/10.3390/ma13081856.

[25] Molod MA, Spyridis P, Barthold F-J. Applications of shape memory alloys in structural engineering with a focus on concrete construction – A comprehensive review. Constr Build Mater 2022;337:127565. https://doi.org/10.1016/J.CONBUILDMAT.2022.127565.

[26] Canbay CA, Karaduman O, Özkul İ. Lagging temperature problem in DTA/DSC measurement on investigation of NiTi SMA. Journal of Materials Science: Materials in Electronics 2020;31:13284–91. https://doi.org/10.1007/s10854-020-03881-y.

[27] Yang S, Su Y, Wang C, Liu X. Microstructure and properties of Cu-Al-Fe high-temperature shape memory alloys. Mater Sci Eng B Solid State Mater Adv Technol 2014;185:67–73. https://doi.org/10.1016/j.mseb.2014.02.001.

[28] Demblon A, Mabe JH, Karaman I. Compositional effects on strain-controlled actuation fatigue of NiTiHf high temperature shape memory alloys. Scr Mater 2024;242:115904. https://doi.org/10.1016/j.scriptamat.2023.115904.

[29] Canbay CA, Karaduman O, Ünlü N, Baiz SA, Özkul İ. Heat treatment and quenching media effects on the thermodynamical, thermoelastical and structural characteristics of a new Cu-based quaternary shape memory alloy. Compos B Eng 2019;174:106940. https://doi.org/10.1016/j.compositesb.2019.106940.

[30] Gao Y, Jian Z. Effect of Cooling Rate on Microstructure, Shape Memory Effect and Mechanical Properties of Cu–13Al–5Fe High-Temperature Shape Memory Alloy Fabricated by Laser Powder Bed Fusion. Transactions of the Indian Institute of Metals 2024;77:1173–9. https://doi.org/10.1007/s12666-023-03236-1.

[31] Zhang X, Liu Q. Cu-Al-Ni-V high-temperature shape memory alloys. Intermetallics (Barking) 2018;92:108–12. https://doi.org/10.1016/j.intermet.2017.10.001.

[32] López-Ferreño I, Gómez-Cortés JF, Breczewski T, Ruiz-Larrea I, Nó ML, San Juan JM. High-temperature shape memory alloys based on the Cu-Al-Ni system: Design and thermomechanical characterization. Journal of Materials Research and Technology 2020;9:9972–84. https://doi.org/10.1016/j.jmrt.2020.07.002.

[33] Tong HC, Wayman CM. Characteristic temperatures and other properties of thermoelastic martensites. Acta Metallurgica 1974;22:887–96. https://doi.org/10.1016/0001-6160(74)90055-8.

[34] Kissinger HE. Reaction Kinetics in Differential Thermal Analysis. Anal Chem 1957;29:1702–6. https://doi.org/10.1021/ac60131a045.

[35] Prado MO, Decorte PM, Lovey F. Martensitic transformation in Cu-Mn-Al alloys. Scripta Metallurgica et Materialia 1995;33. https://doi.org/10.1016/0956-716X(95)00292-4.

[36] Chentouf SM, Bouabdallah M, Gachon JC, Patoor E, Sari A. Microstructural and thermodynamic study of hypoeutectoidal Cu-Al-Ni shape memory alloys. J Alloys Compd 2009;470:507–14. https://doi.org/10.1016/j.jallcom.2008.03.009.

[37] Chentouf SM, Bouabdallah M, Cheniti H, Eberhardt A, Patoor E, Sari A. Ageing study of Cu–Al–Be hypoeutectoid shape memory alloy. Mater Charact 2010;61. https://doi.org/10.1016/j.matchar.2010.07.009.

[38] Pelegrina JL, Ahlers M. The martensitic phases and their stability in Cu□Zn and Cu□Zn□Al alloys—I. The transformation between the high temperature β phase and the 18R martensite. Acta Metallurgica et Materialia 1992;40. https://doi.org/10.1016/0956-7151(92)90033-B.

[39] Saud SN, Hamzah E, Abubakar T, Bakhsheshi-Rad HR. Thermal aging behavior in Cu-Al-Ni-xCo shape memory alloys. J Therm Anal Calorim 2015;119:1273–84. https://doi.org/10.1007/s10973-014-4265-6.

[40] Wang H, Huang J, Chen S, Yuan X, Zhu J, Xu D, et al. Microstructure and shape memory properties of Cu-Al-Fe alloys with different Al contents made by additive manufacturing technology. Mater Res Express 2022;9:095701. https://doi.org/10.1088/2053-1591/ac8d4f.

[41] Raju TN, Sampath V. Influence of aluminium and iron contents on the transformation temperatures of Cu-Al-Fe shape memory alloys. Transactions of the Indian Institute of Metals 2011;64:165–8. https://doi.org/10.1007/s12666-011-0032-6.

[42] Patterson AL. The Scherrer Formula for I-Ray Particle Size Determination. Physical Review 1939;56:978–82. https://doi.org/10.1103/PhysRev.56.978.